Robust Fault Diagnosis for Quadrotor UAVs Using Adaptive Thau Observer

Zhaohui Cen · Hassan Noura · Tri Bagus Susilo · Younes Al Younes

Abstract A robust Fault Diagnosis (FD) scheme for a real quadrotor Unmanned Aerial Vehicle (UAV) is proposed in this paper. Firstly, a novel Adaptive Thau observer (ATO) is developed to estimate the quadrotor system states and build a set of offset residuals to indicate actuators' faults. Based on these residuals, some rules of Fault Diagnosis (FD) are designed to detect and isolate the faults as well as estimate the fault offset parameters. Secondly, a synthetic robust optimization scheme is presented to improve Fault Estimation (FE) accuracies, three key issues include modeling uncertainties, and magnitude order unbalances as well as noises are addressed. Finally, a typical fault of rotors is simulated and injected into one of four rotors of the quadrotor, and experiments for the FD scheme have been carried out. Unlike former research works on the FD schemes for quadrotors, our proposed FD scheme based on the ATO can not only detect and isolate the failed actuators, but also estimate the fault severities. Regardless of roughness of the real flying data, the FD results still have sufficient FE accuracies.

Keywords Adaptive Thau observer · Quadrotor · Fault detection · Isolation and estimation · Robustness

Z. Cen · H. Noura (✉) · T. B. Susilo · Y. Al Younes
Department of Electrical Engneering,
UAE University, Al Ain, UAE, 15551
e-mail: hnoura@uaeu.ac.ae

Z. Cen
e-mail: cenzhaohui@gmail.com

T. B. Susilo
e-mail: tribagus@uaeu.ac.ae

Y. Al Younes
Mechanical Engineering Faculty, Higher College of Technology, Al Ain, UAE, 17155
e-mail: yalyounes@hct.ac.ae

1 Introduction

Small unmanned aerial vehicle (UAV) quadrotors are designed to easily move in different environments while following specific tasks and providing a good performance as well as a great autonomy [1–3]. As an example of UAV systems, the quadrotor helicopter is fairly an easy, affordable and easy-to-fly system [4, 5]. Therefore, it has been widely used to develop, implement and test-fly methods in control [6, 7], object tracking [8–10], fault diagnosis [1], fault tolerant control as well as multi-agent based techniques in formation flight [11], remote monitoring, and communications.

Affected by aerodynamic forces, the quadrotor dynamics is nonlinear, multivariable, and is

subject to component failures and external disturbances with different severities. In turn, some necessary safety measures for the quadrotor are required, corresponding to different safety level requirement. First of all, the quadrotor flight control system should be at least fault-tolerant under some failures. Secondly, more active and effective Fault Tolerant Control (FTC) should be designed for high-efficiency safety maintenances. Finally, as a precondition of the active FTC, fault estimation coping with fault detection and isolation needs to be addressed for the effectiveness of active FTC.

Studies on Fault Diagnosis (FD) and FTC of quadrotor UAVs increased rapidly in recent years in order to make UAVs fly safely. Generally, FTC can be classified as passive FTC and active FTC. Currently, a lot of works introduce FTC of quadrotors, especially passive FTC [12–14]. The passive FTC has the advantage that the knowledge about fault is not required, but the fault-tolerant capacity is limited [15]. Compared with the passive FTC, the active FTC has better fault-tolerant capacity and provide necessary Condition-Based Maintains for object system [16]. Therefore, the active FTC has attracted more attentions and become a hotspot problem in the current research field of FTC. Actually, because FD is an essential precondition for active FTC, many researches on Active FTC will suppose the FD result has been given or some researches only address the FD problem as their principal contributions.

Freddi et al. [1–3] proposed a model-observer based FD scheme, it can detect sensor and actuator faults based on a set of observer residuals, but the residuals are inaccurate and not applicable for fault isolation and estimation. Moreover, the model-observer based FD method is only applicable for quadrotor models but not real quadrotors. Although the former research works make some contributions on FD and FTC, most of them supposed that the FD results have been given, or are only validated for quadrotor models, and few researches on FD for real quadrotors is proposed and also validated based on the flying data of real quadrotors. Zhang at el. has done a lot of works on FD methods for the active FTC for quadrotors [17–19]. Ma and Zhang also proposed another FE method for quadrotors based on Two Stage Extended Kalman Filter (TSEKF) and Dual Unscented Kalman Filter (DUKF) [20–22], which can estimate the system states and parameters at the same time. But, the EKF-based FD method has an inherit drawback on linearization for nonlinear object system. Also, the EKF-based FD method are not robust for noise and have rough FD results if the transfer matrices in EKF are not sufficient accurate. Ranjbaran and Khorasani [23] proposed an adaptive observer to estimate the fault parameter in actuators, where the active FTC based on model reference control can compensate for the fault. However, the works mentioned above are simulated but not implemented on real quadrotors. A FE scheme using ATO for a real quadrotor is initially proposed in our former work [24], but the FE results were inaccurate and rough due to the presence of uncertainties, disturbances, and noises during flight tests of the real quadrotor.

The contribution of this work consists of proposing a novel ATO based FD scheme for a real quadrotor faults. And also a synthetic robust optimization FE scheme is presented to obtain a better FE. The problems such as unmodeled nonlinearities, magnitude order unbalances and disturbances, which are subject to rotor faults, are well solved. Compared with the latest work on FD for quadrotors using thau observers [1–3], the original thau observer is improved to be applicable for FE. Unlike former research works on FD for quadrotors, our FD scheme is applicable for real flight data, but it still has sufficient accuracies of FD. Compared to our former work in [24, 25], the uncertain elements in real experiment are considered, a novel optimization FE scheme is proposed to solve these problems. And the FE result is obviously improved.

This paper is organized as follows. In Section 2, the quadrotor model and robust FD problems are presented. The proposed FD scheme based on nonlinear Thau observer is described in Section 3. The proposed robust FE scheme based on ATO and three optimization measures are presented in Section 4. Section 5 is devoted to the presentation of the experiment results obtained for the fault scenarios when the proposed scheme is applied to the quadrotor. Finally, conclusions are presented in Section 6.

2 Quadrotor and Problem Formulation

2.1 Quadrotor Kinematic and Dynamics

The dynamic model of light-weight aircraft systems includes the gyroscopic effects resulting from both the rigid body rotation in space, and the four propeller's rotation. The model is derived from the Euler-Lagrange formalism. A body-fixed frame B and the earth-fixed frame E are assumed to be at the center of gravity of the quadrotor UAV, where the z-axis is pointing upwards, as seen in Fig. 1.

The position of the quadrotor UAV in earth frames is given by a vector (x, y, z). The orientation of a quadrotor UAV that referred to as roll, pitch, and yaw is given by a vector (ϕ, θ, ψ) which is measured with respect to the earth coordinate frame E [2].

The vectors transformation from frame B to frame E can be calculated based on Euler angles and the rotation matrix R_{EB}.

$$R_{EB}$$
$$= \begin{bmatrix} C_\psi C_\theta & -S_\psi C_\phi + C_\psi S_\theta S_\phi & S_\psi S_\phi + C_\psi S_\theta C_\phi \\ S_\psi C_\theta & C_\psi C_\phi + S_\psi S_\theta S_\phi & -C_\psi S_\phi + S_\psi S_\theta C_\phi \\ -S_\theta & C_\theta S_\phi & C_\phi C_\theta \end{bmatrix}$$
$$(1)$$
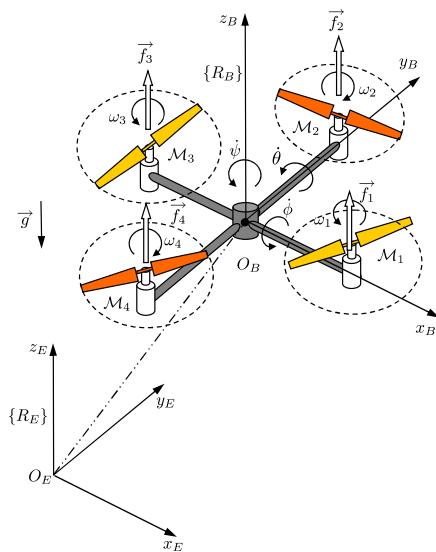
Fig. 1 The quadrotor in different frames

Where $S(\cdot)$ and $C(\cdot)$ have been denoted as $\sin(\cdot)$ and $\cos(\cdot)$, respectively. It should be noted that $R_{EB} = R_{BE}^T$.

The thrust force from rotor $i, i = 1, 2, 3, 4$ is $F_i = b\omega_i^2$. Where b is the thrust factor and ω_i is the rotor speed. In the body-fixed frame B, the outside forces are defined as follows:

$$F_B = \begin{bmatrix} F_{xB} \\ F_{yB} \\ F_{zB} \end{bmatrix} = \begin{bmatrix} 0 \\ 0 \\ \sum_{i=1}^4 F_i \end{bmatrix} \quad (2)$$

The forces in the earth-fixed frame can be denoted as:

$$\begin{bmatrix} F_x \\ F_y \\ F_z \end{bmatrix} = R_{EB}.F_B$$

$$= \left(\sum_{j=1}^4 F_j \right) \begin{bmatrix} S_\psi S_\phi + C_\psi S_\theta C_\phi \\ -C_\psi S_\phi + S_\psi S_\theta C_\phi \\ C_\phi C_\theta \end{bmatrix} \quad (3)$$

Therefore, the motion equation in the earth fixed frame can be represented as:

$$m \begin{bmatrix} \ddot{x} \\ \ddot{y} \\ \ddot{z} \end{bmatrix} = \begin{bmatrix} F_x - K_1\dot{x} \\ F_y - K_2\dot{y} \\ F_z - mg - K_3\dot{z} \end{bmatrix}$$

$$= \begin{bmatrix} \sum_{j=1}^4 F_j \left(C_\psi S_\theta C_\phi + S_\psi S_\phi \right) - K_1\dot{x} \\ \sum_{j=1}^4 F_j \left(S_\psi S_\theta C_\phi - C_\psi S_\phi \right) - K_2\dot{y} \\ \sum_{j=1}^4 F_j C_\theta C_\phi - mg - K_3\dot{z} \end{bmatrix} \quad (4)$$

where K_i $(i = 1, 2, 3)$ is the drag coefficient of corresponding axis. Note that these coefficients can be negligible at low speed.

The dynamic model of quadrotors also contains the gyroscopic effect resulting from the rigid body rotation, the gyroscopic effect resulting from the propeller rotation coupled with the body rotation, the actuators action and finally the drag effects. Using the Lagrangian method, quadrotor rotational dynamic model is as follows [26]:

$$\ddot{\phi} = (\dot{\theta}\dot{\psi}(I_y - I_x) - J\dot{\theta}\omega + lU_1)/I_x - K_4\dot{\phi}$$
$$\ddot{\theta} = (\dot{\phi}\dot{\psi}(I_z - I_x) + J\dot{\phi}\omega + lU_2)/I_y - K_5\dot{\theta} \quad (5)$$
$$\ddot{\psi} = (\dot{\phi}\dot{\theta}(I_x - I_y) + U_3)/I_z - K_6\dot{\psi}$$

Where K_i is the drag coefficient, and the system's inputs U_1, U_2, U_3, U_4 are defined as follows:

$$U_1 = b \left(\omega_4^2 - \omega_3^2 \right) = F_4 - F_3$$

$$U_2 = b \left(\omega_2^2 - \omega_1^2 \right) = F_2 - F_1$$

$$U_3 = d \left(\omega_1^2 + \omega_2^2 - \omega_3^2 - \omega_4^2 \right)$$

$$U_4 = b \left(\omega_1^2 + \omega_2^2 + \omega_3^2 + \omega_4^2 \right) = \sum_{i=1}^{4} F_i \quad (6)$$

Where b and d are the thrust and drag factor respectively, and $\omega = \omega_4 + \omega_3 - \omega_2 - \omega_1$ is considered as a disturbance.

The relationship between system's inputs and rotors' speed can be described as follows:

$$\begin{bmatrix} U_1 \\ U_2 \\ U_3 \\ U_4 \end{bmatrix} = \begin{bmatrix} 0 & 0 & -b & b \\ -b & b & 0 & 0 \\ d & d & -d & -d \\ b & b & b & b \end{bmatrix} \begin{bmatrix} \omega_1^2 \\ \omega_2^2 \\ \omega_3^2 \\ \omega_4^2 \end{bmatrix} = \Omega \begin{bmatrix} \omega_1^2 \\ \omega_2^2 \\ \omega_3^2 \\ \omega_4^2 \end{bmatrix}$$
$$(7)$$

Since Ω is nonsingular, for each U_1 we can find appropriate ω_j^2, $j = 1, \ldots, 4$ while the other inputs U_k, $k \neq i$ do not change.

2.2 Problem Formulation

2.2.1 Fault Diagnosis and Fault Estimation

In order to simulate the fault effect under real scenarios while the quadrotor cannot be damaged, a partial loss of rotor effectiveness is generally simulated and injected into the test bed. The fault scenario is to inject fault into one of the four rotors, and the gain of the corresponding rotor driver command signal decreases instead of a real performance decrease.

Defining $x = \left(\phi, \theta, \psi, \dot{\phi}, \dot{\theta}, \dot{\psi} \right)$ as the state vector, $u = \begin{bmatrix} U_\phi & U_\theta & U_\psi \end{bmatrix}$ as the input vector and $y = \begin{bmatrix} \phi & \theta & \psi \end{bmatrix}^T$ as the output vector, the system described by Eq. 5 can be rewritten in the state-space form $\dot{x} = f(x, u)$ as:

$$\begin{cases} \dot{x}(t) = Ax(t) + Bu(t) + H(x(t), u(t)) \\ y(t) = Cx(t) \end{cases} \quad (8)$$

Where $H(x, u) = \begin{bmatrix} 0 & 0 & 0 & h(x, u)^T \end{bmatrix}^T$ and

$$h(x, u) = \begin{bmatrix} \dot{\psi}\dot{\theta} \left(I_y - I_z / I_x \right) - J\dot{\theta}\omega / I_x \\ \dot{\phi}\dot{\psi} \left(I_z - I_x / I_y \right) + J\dot{\phi}\omega / I_y \\ \dot{\theta}\dot{\phi} \left(I_x - I_y / I_z \right) \end{bmatrix} \quad (9)$$

When an actuator fault occurs, the faulty system can be given by Eq. 10, which is derived from Eq. 8:

$$\begin{cases} \dot{x}(t) = Ax(t) + Bu(t) \\ \quad + H(x(t), u(t)) + Ff(t) \\ y(t) = Cx(t) \end{cases} \quad (10)$$

Where F is known as the fault entry matrix, which represents the effect of faults on the system. The objective is to detect, isolate and even estimate the fault severity. So, in order to design and implement an active FTC approach for quadrotors, it is essential to propose a solution to detect and estimate the fault magnitude f in Eq. 10.

2.2.2 Uncertainties with Effects on FE

Equations 8–10 describe the dynamic behavior in the format of state-space equations, but it does not match with the real quadrotor behaviors during experiments, because the real quadrotor has more uncertainties such as complex couple dynamics and unknown inputs. Affected by these uncertainties, the FE residuals are very rough when the original ATO is used to estimate the actuator fault of the real quadrotor. Generally, the residuals are used to indicate whether a fault occurs or does not occur. In other words, the values of residuals should be theoretically zero in case of faults, but actually it is not zero because of the influence from the uncertainties which include model uncertainties, magnitude order unbalance, and noise.

Firstly, the modeling uncertainties come from the unmatched dynamics and nonlinearities between the model used in the ATO and the dynamics of a real quadrotor system. Generally, the attitude control model given in Eq. 5 is used to model the quadrotor. But, the terms $K_4\dot{\phi}$, $K_5\dot{\theta}$ and $K_6\dot{\psi}$ are omitted in model observer design because, in quadrotor model simulations, these terms are often neglected or considered as constant. If this state observer is used again to estimate the states
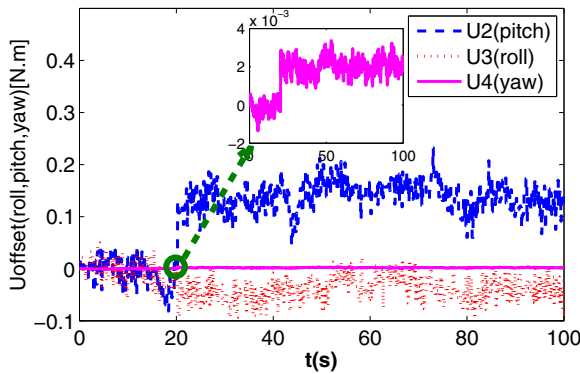
Fig. 2 Fault offset value comparison

of the real quadrotor, these terms should be added into the observer and the parameters should be identified.

Secondly, the magnitude order unbalance means the torque values of the roll and pitch have different orders of magnitude from the one of the yaw. That is because the rotor faults have different effect on roll, pitch and yaw controls. As can be seen from Fig. 2, the value of U2 (roll) and U3 (pitch) are around 10e-2, while the value of U4 (pitch) is around 10e-3. The different magnitude orders of the three torques value will result in that the observer estimation errors follow the larger magnitude order 10e-2 because of its inherent estimation error for adaptive update law.

Thirdly, as a result of low-efficiency of sensors, the measurement values provided by the sensors are affected by noise. And also the noise in residuals comes from the noise in control inputs U1–U4 and the noise in sensors ϕ, θ, φ.

Based on the problems stated above, it is essential to analyze the FE and its robust optimization approach for high-accurate FD and effective active FTC.

3 FD Based on Nonlinear Observer

3.1 Fault Detection Based on Thau Observer

With reference to Eq. 10, the following conditions must be satisfied for the observer design:

C1 the pair(C,A) is observable;

C2 the nonlinear function $h(x, u)$ must be continuously differentiable and locally Lipschitz with constant ρ, i.e.

$$\|h(x_1(t), u(t)) - h(x_2(t), u(t))\| \le \rho \|(x_1 - x_2)\| \tag{11}$$

If these two conditions hold, a nonlinear thau observer can be constructed as:

$$\begin{cases} \dot{\hat{x}}(t) = A\hat{x}(t) + Bu(t) + H(\hat{x}(t), u(t)) \\ \quad + K(y(t) - \hat{y}(t)) \\ \hat{y}(t) = C\hat{x}(t) \end{cases} \tag{12}$$

Where **K** is the thau observer gain matrix, and is obtained based on Lemma 1.

Lemma 1 *If the gain matrix in Eq.* 12 *satisfies* [2]*:*

$$K = P_\theta^{-1} C^T \tag{13}$$

And matrix P_θ is the solution to the Lyapunov equation

$$A^T P_\theta + P_\theta A - C^T C + \theta C^T P_\theta = 0 \tag{14}$$

Where θ is a positive parameter which is chosen such that Eq. 14 *has a positive definite solution, then the state of Eq.* 12 *is an asymptotic estimation of the system state described by Eq.* 8*, that is,*

$$\lim_{t \to \infty} e(t) = \lim_{t \to \infty} (x(t) - \hat{x}(t)) = 0 \tag{15}$$

In this case of study the pair (C,A) is observable and the first condition is easy to be satisfied. Since h(x(t),u(t)) is a function with only multiplications and divisions. it is continuously differentiable and thus the condition C2 holds if u is properly chosen. The parameter θ can be chosen in order to maximize the fault effect on the residuals while keeping the FD time small.

3.2 FD Based on Adaptive Thau Observer

In order to isolate the fault, the thau observer is improved to estimate the offset residual of actuator faults. Based on the fault detection result

from thau observer, an adaptive thau observer is proposed to estimate the fault severity. With reference to Eq. 10, a novel thau observer can be constructed as:

$$
\begin{cases}
\dot{\hat{x}}(t) = A\hat{x}(t) + Bu(t) + H(\hat{x}(t), u(t)) \\
\quad + F_1 \hat{f}(t) + K(y(t) - \hat{y}(t)) \\
\hat{y}(t) = C\hat{x}(t)
\end{cases}
\tag{16}
$$

Where $\hat{x}(t) \in R^n$ is the observer state vector, $\hat{y}(t) \in R^p$ is the observer output vector and $\hat{f}(t)$ is an estimation of $f(t)$. $K \in R^{n \times p}$ is the observer gain.

Denote the estimation error as $e_x(t) = x(t) - \hat{x}(t)$, the estimation error dynamics is described by

$$
\dot{e}_x(t) = (A - KC) e_x(t) + [H(x) - H(\hat{x})] \\
\quad + F e_f(t)
\tag{17}
$$

Where the fault estimation error is denoted as $e_f(t) = f(t) - \hat{f}(t)$.

The purpose of the proposed adaptive thau observer is not only to detect faults, but also to estimate the fault parameters, which can be used for active FTC.

Theorem 1 *For the available observer gain K in Theorem 1 and a given matrix $Q_{(n \times n)} > 0$ and a positive parameter γ, if there exist two matrices $P_{n \times n}$ and $G_{r \times p}$, such that*

$$
P(A - KC) + (A - KC)^T P + \gamma PP + \gamma I = -Q
\tag{18}
$$

$$
PB = C^T G^T
\tag{19}
$$

Then the observer is described by Eq. 16 and the following adaptive fault estimation algorithm [27, 28]

$$
\dot{\hat{f}}(t) = \Gamma G(y(t) - \hat{y}(t)) - \sigma \Gamma \hat{f}(t)
\tag{20}
$$

can realize $\lim\limits_{t \to \infty} e_x(t) = 0$ and $\lim\limits_{t \to \infty} e_f(t) = 0$, where $\Gamma = \Gamma^T > 0$, and σ is positive constant factor satisfying $\sigma - \lambda_{\max}(\Gamma^{-1}) > 0$, $\lambda_{\max}(\cdot)$ is the maximum eigenvalue of the corresponding matrix.

Proof From $e_f(t) = f(t) - \hat{f}(t)$, the derivative of $e_f(t)$ can be given by

$$
\dot{e}_f = \dot{f} - \Gamma G e_y + \sigma \Gamma f - \sigma \Gamma e_f
\tag{21}
$$

Consider the following Lyapunov function

$$
V(t) = e_x^T P e_x + e_f^T \Gamma^{-1} e_f
\tag{22}
$$

Then its derivative is

$$
\begin{aligned}
\dot{V} &= e_x^T \left[(A - LC)^T P + P(A - LC) \right] e_x \\
&\quad + 2e_x^T P \left[H(x) - H(\hat{x}) \right] \\
&\quad + 2e_f^T \Gamma^{-1} \dot{f} + 2\sigma e_f^T f - 2\sigma e_f^T e_f \\
&\leq e_x^T \left[(A - LC)^T P + P(A - LC) + \gamma PP + \gamma I \right] e_x \\
&\quad + \lambda_{\max}(\Gamma^{-1}) \cdot \left[\|e_f\|^2 + f_1^2 \right] \\
&\quad + \sigma \left[\|e_f\|^2 + f_0^2 \right] - 2\sigma \|e_f\|^2 \\
&\leq -\lambda_{\min}(Q) \cdot \|e_x\|^2 - \left[\sigma - \lambda_{\max}(\Gamma^{-1}) \right] \cdot \|e_f\|^2 \\
&\quad + \lambda_{\max}(\Gamma^{-1}) \cdot f_1^2 + \sigma f_0^2 \\
&= -\lambda_{\min}(Q) \cdot \|e_x\|^2 - \left[\sigma - \lambda_{\max}(\Gamma^{-1}) \right] \cdot \|e_f\|^2 + \beta
\end{aligned}
\tag{23}
$$

Where $\beta = \lambda_{\max}(\Gamma^{-1}) \cdot f_1^2 + \sigma f_0^2$; $\lambda_{\min}(\cdot)$ is the minimum eigenvalue of the corresponding matrix. If the appropriate parameters are chosen such that

$$
\sigma - \lambda_{\max}(\Gamma^{-1}) > 0
\tag{24}
$$

Then $\dot{V}$ can be written as

$$
\dot{V} \leq -\min \left[\lambda_{\min}(Q), \sigma - \lambda_{\max}(\Gamma^{-1}) \right] \\
\quad \cdot \left(\|e_x\|^2 + \|e_f\|^2 \right) + \beta
\tag{25}
$$

Where min(.) denotes the minimum value of a set of numbers. Again, from $V(t) = e_x^T P e_x + e_f^T \Gamma^{-1} e_f$ it can be obtained:

$$
V \leq \max \left[\lambda_{\max}(P), \lambda_{\max}(\Gamma^{-1}) \right] \cdot \left(\|e_x\|^2 + \|e_f\|^2 \right)
\tag{26}
$$

Where max(.) denotes the maximum one of a set. Thus

$$
\dot{V} \leq -\alpha V + \beta
\tag{27}
$$

Where $\alpha = \frac{\min[\lambda_{\min}(Q), \sigma - \lambda_{\max}(\Gamma^{-1})]}{\max[\lambda_{\max}(P), \lambda_{\max}(\Gamma^{-1})]}$. The differential inequality (27) satisfies $0 \leq V(t) \leq \frac{\beta}{\alpha} + [V(0) - \frac{\beta}{\alpha}] e^{-\alpha t}$, so as $t \to \infty$, $V(t)$ is bounded. Therefore, the proposed ATO is asymptotically stable; e_f is also ultimately bounded. The ultimate norm bound of e_f can be easily calculated out:

$$\|e_f\| \leq \sqrt{\frac{\beta}{\alpha \lambda_{\min}(\Gamma^{-1})}} \tag{28}$$

This completes the proof.   □

Remark 1 Theorem 1 is suitable for all faults with different time-varying natures theoretically. However, it should be pointed that the estimation convergence speed depends both on the fault time-varying natures and the specified parameters of ATO. Hereby as can be seen from Eq. 21, a suitable values of Γ and σ should be set for better estimation performance subject to faults with different time-varying natures.

3.3 Fault Isolation and Fault Estimation Rules

In a real implementation, disturbances and unknown inputs may affect the fault estimation $\hat{f}(t)$ which may not be accurate. The FD procedure for a real implementation is depicted in Fig. 3. The fault detection based on thau observer firstly activates the ATO under a fault situation; The ATO will get the estimation for the fault offset value. Depending on the estimation accuracy, FD includes isolation and even estimation is given.
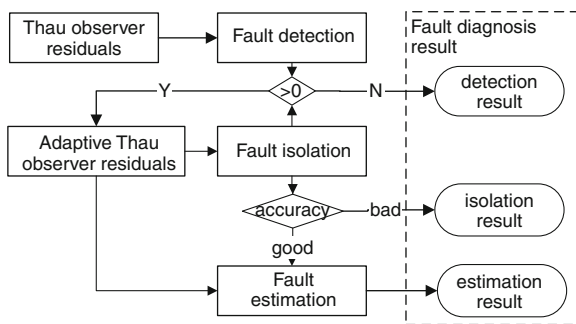
Fig. 3 FD procedure plot of engineering implement for quadrotor faults

4 Robust FE Using Optimized ATO

Based on the three uncertainties about modeling uncertainties, data unbalance and noise, the original ATO is improved and optimized by a synthetic approach with three steps. The first step is compensating for the uncertainties based on parameters identification; the second step is amplifying and reducing the magnitude orders to avoid magnitude order unbalance; the third step is filtering the noise using a specified low-pass filter.

4.1 Modeling Uncertainties Analysis and Parameter Identification

It should be pointed that the nonlinearity terms $h(x,u)$ in ATO should be in the format of Eq. 29 for a better estimation.

$$h(x,u) = \begin{bmatrix} \dot{\psi}\dot{\theta}(I_y - I_z/I_x) - J\dot{\theta}\omega/I_x - K_4\dot{\phi} \\ \dot{\phi}\dot{\psi}(I_z - I_x/I_y) + J\dot{\phi}\omega/I_y - K_5\dot{\theta} \\ \dot{\theta}\dot{\phi}(I_x - I_y/I_z) - K_6\dot{\psi} \end{bmatrix} \tag{29}$$

But it is generally simplified in practice as stated in Eq. 9 because the drag terms $K_4\dot{\phi}$, $K_5\dot{\theta}$, $K_6\dot{\psi}$ and the coupling terms $J\dot{\theta}\omega/I_x$, $J\dot{\phi}\omega/I_y$ can be compensated by the observer feedback gain and then omitted. However, for real quadrotor flight data, these terms cannot be omitted and the nonlinear terms of $h(x,u)$ in ATO should be in the format of Eq. 29 instead of Eq. 9.

The coupling terms $J\dot{\theta}\omega/I_x$ and $J\dot{\phi}\omega/I_y$ are easy to be augmented because the parameters I_x, I_y and J can be obtained experimentally. But the drag terms K_4, K_5 and K_6 are unknown and their values depend on test flight conditions.

Based on this issue, a parameter identification scheme is designed as below.

$$\hat{K}_{[4,5,6]} = ident < e_f, [\dot{\phi}, \dot{\theta}, \dot{\psi}] > \tag{30}$$

where a linear regression is utilized to identify the parameters, and the identification parameters $\hat{K}_{[4,5,6]}$ are substituted in Eq. 29 instead of the real parameters $K_{[4,5,6]}$.

4.2 Data Adjustment Based on Amplifying and Reducing

As can be seen from Fig. 2, the thrust of yaw has a smaller magnitude order 10^{-3} compared to the thrusts of roll and pitch. The FE for yaw has a relatively large error, although the error is same as the ones for roll and pitch because the convergence nature of the ATO. In order to overcome the problem of magnitude order unbalance, an improvement on the ATO using amplifying and reducing is proposed below.

Based on Eq. 5, the input vector $u = \begin{bmatrix} u_\phi & u_\theta & u_\psi \end{bmatrix}^T$, can be obtained from the transformation calculation of the measurable outputs of the controller. This input vector u is sent into the ATO to estimate the fault offset $f = \begin{bmatrix} f_\phi & f_\theta & f_\psi \end{bmatrix}^T$. In order to make the data magnitude of the three channels varying in the same range and keep the balance, the system input u is modified as follows:

$$u = \begin{bmatrix} u_\phi & u_\theta & gu_\psi \end{bmatrix}^T \tag{31}$$

Where g is an adjustment gain factor to make gu_ψ have the same magnitude order with u_ϕ and u_θ. As a result of the change for the input of yaw, the parameters of the observer feedback gain and adaptive law for yaw control should be updated to keep its convergence of yaw control. So Theorem 2 is proposed for the new estimation.

Theorem 2 *If a new estimation $\hat{f}_\psi^{new}$ can be obtained based on the ATO while f_ϕ and f_θ are same as before and the former FE of yaw control is defined as $\hat{f}_\psi$, it should be followed as below according to the analytical relationship in Eq. 5:*

$$\hat{f}_\psi^{new} = g\hat{f}_\psi \tag{32}$$

Proof The result above can be deducted as below. The dynamics of the ATO is described as

$$\dot{\hat{x}}(t) = A\hat{x}(t) + Bu(t) + H\left(\hat{x}(t), u(t)\right)$$
$$+ F_1\hat{f}(t) + K\left(y(t) - \hat{y}(t)\right) \tag{33}$$

If the observer converges and the system is stable, then that the following is satisfied: $\dot{\hat{x}}(t) =$

0, $\hat{x}(t) = 0$ and $y(t) - \hat{y}(t) = 0$. So the fault estimation $\hat{f}$ is such that:

$$Bu(t) + H\left(\hat{x}(t), u(t)\right) + F_1\hat{f}(t) = 0 \tag{34}$$

For the yaw control, the dynamics can be denoted as

$$u_\psi + \dot{\theta}\dot{\phi}\left(I_x - I_y/I_z\right) - K_6\dot{\psi} + \hat{f} = 0 \tag{35}$$

Since the terms $\dot{\theta}\dot{\phi}\left(I_x - I_y/I_z\right)$ and $-K_6\dot{\psi}$ should be zero under small-angle flying or stable conditions, it can be obtained as:

$$u_\psi = -\hat{f} \tag{36}$$

So if $u_\psi^{new} = gu_\psi$, and then $\hat{f}_\psi^{new} = g\hat{f}_\psi$.

After the new estimation is obtained from the new ATO, the desired real FE value can be obtained by reducing the estimation with same gain as below:

$$\hat{f}_\psi = \hat{f}_\psi^{new}\Big/ g \tag{37}$$

$\square$

Remark 2 Theoretically, this improvement based on amplifying and reducing does not change the analytical relationship for the observer estimation. But it is useful to reduce the magnitude orders of errors and decrease the estimation errors, which can be demonstrated by the experiment comparison in Section 5.

4.3 Noise Filtering

The noises for FE are mainly issued from measurement noises and random disturbances, which take effects on both actuator control inputs and sensor measurement outputs.

Based on statistical characters of the signal in frequency spectrum and for the sake of simplicity of the digital signal processing filter structure, a low-pass IIR filter is utilized to filter the noise and decrease the complexity of the digital signal processing, which is shown in Fig. 4.

As can be seen from Fig. 4, six channel signals are sent into the IIR filters before being sent into the ATO for FE. Because the six channel signals have different frequency spectrum, it is necessary
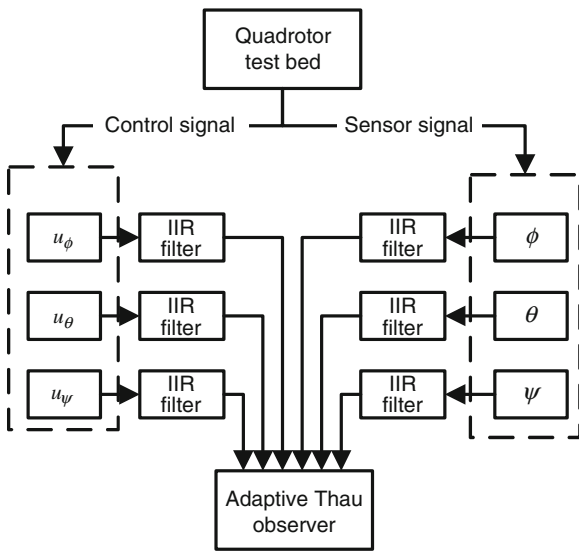
Fig. 4 Filtering process for monitoring data

Fig. 5 The quadrotor test bed

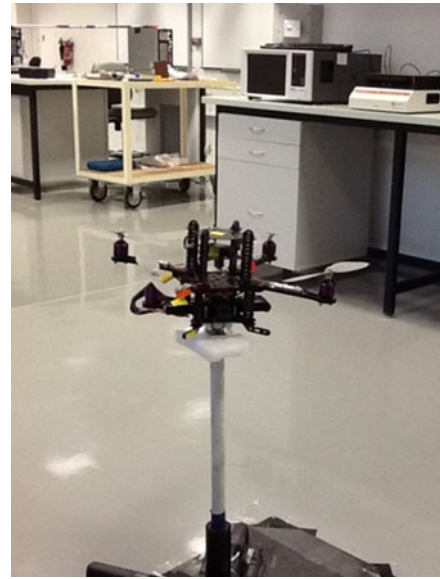to specify different filter parameters to get the best denoising result.

5 Experiment

In order to show the performance and the efficiency of the fault detection and fault estimation, the proposed ATO approach and robust optimization method in the real quadrotor test bed environment is tested.

5.1 Test Bed Setup and Parameters Specification

With consideration for research objective and safe-flying, a quadrotor test bed is developed in the control lab of UAEU shown in Fig. 5. From a PC and through a USB port link, the firmware compiled by Matlab/Simluink RTW can be downloaded into the quadrotor microcontroller, and then the remote control is operated to switch from the manual control mode into the automatic control mode. During the flight of the quadrotor, the control measurement and sensor data are sent to PC through a zigbee wireless communication link. All the work procedures above are depicted in Fig. 6.

The quadrotor model, which parameters are identified from a real quadrotor is used in this

paper. The parameters of the quadrotor are below:

$$m = 1 \text{ kg},$$
$$I_{xx} = 8.1 \times 10^{-3} \text{ N.m/rad}/s^2,$$
$$I_{yy} = 8.1 \times 10^{-3} \text{ N.m/rad}/s^2,$$
$$I_{zz} = 14.2 \times 10^{-3} \text{ N.m/rad}/s^2,$$
$$g = 9.81 \text{ m}/s^2,$$
$$J = 104 \times 10^{-6} \text{ N.m/rad}/s^2.$$
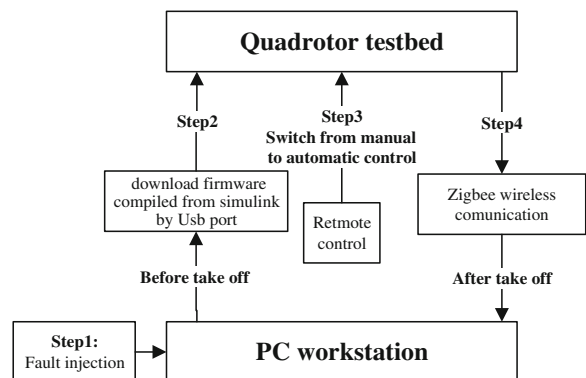
Fig. 6 Fault injection and flying test flowchart

$$A = \begin{bmatrix} 0_{6 \times 6} & I_{6 \times 6} \\ 0_{6 \times 6} & 0_{6 \times 6} \end{bmatrix},$$

$$B = \begin{bmatrix} 0_{9 \times 1} & 0_{9 \times 3} \\ 0_{3 \times 1} & I_{3 \times 3} \end{bmatrix},$$

$$C = \begin{bmatrix} I_{6 \times 6} & 0_{6 \times 6} \end{bmatrix},$$
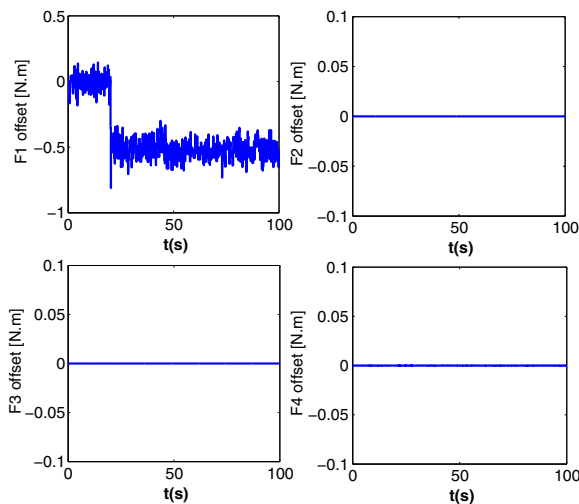
The parameters of the observers are below:

$$K = \begin{bmatrix} 1.1 & 0 & 0 \\ 0 & 1.1 & 0 \\ 0 & 0 & 1.1 \\ 0.3205 & 0 & 0 \\ 0 & 0.3205 & 0 \\ 0 & 0 & 0.3205 \end{bmatrix}$$

$$G = \begin{bmatrix} 5.38 & 0 & 0 \\ 0 & 5.38 & 0 \\ 0 & 0 & 5.38 \end{bmatrix}$$

$\Gamma = I_4 \times 10^{-8} \ \sigma = 2 \times 10^8$.

The classical PID control law for attitude and altitude control is introduced to control the quadrotor to a specified operating point. Figure 6 shows the control trajectory of the attitude with the set operating point $[\phi, \theta, \varphi]_o = [0rad, 0rad, \pi/4rad]$ and the initial position $[\phi, \theta, \varphi]_i = [0rad, 0rad, 0rad]$

A Partial Loss of Effectiveness(LOE) by 30 % is injected into rotor F1, the offset value of rotors resulting from the fault is shown in Fig. 7.


**Fig. 8** U1–U4 with fault and without fault

Comparisons between the controller output U1–U4 with fault and the ones without fault are shown in Fig. 8. As can be seen from Fig. 7, only rotor thrust F1 decreases while the other three rotors' thrusts keep zero. As can be seen from Fig. 8, U1, U3, U4 changes because all the three control output are linked to F1.

5.2 Fault Diagnosis Result

The attitude angles during the flight are shown in Fig. 9. Comparisons among the control output U before the fault- U_{bf}, the estimation of controller

Fig. 7 Rotors' offset by the fault
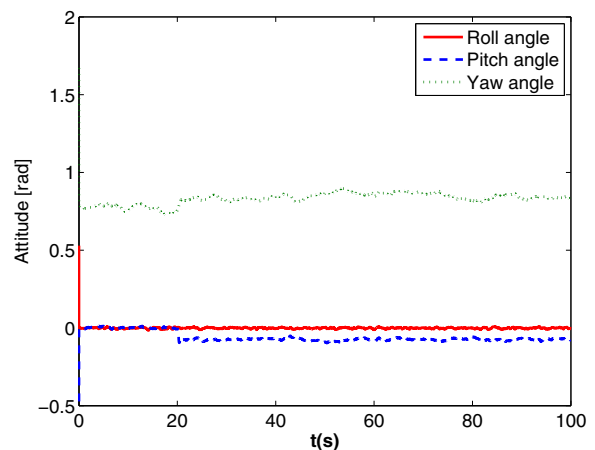
Fig. 9 The attitude angles

Fig. 10 Comparisons among *roll*, *pitch* and *yaw*
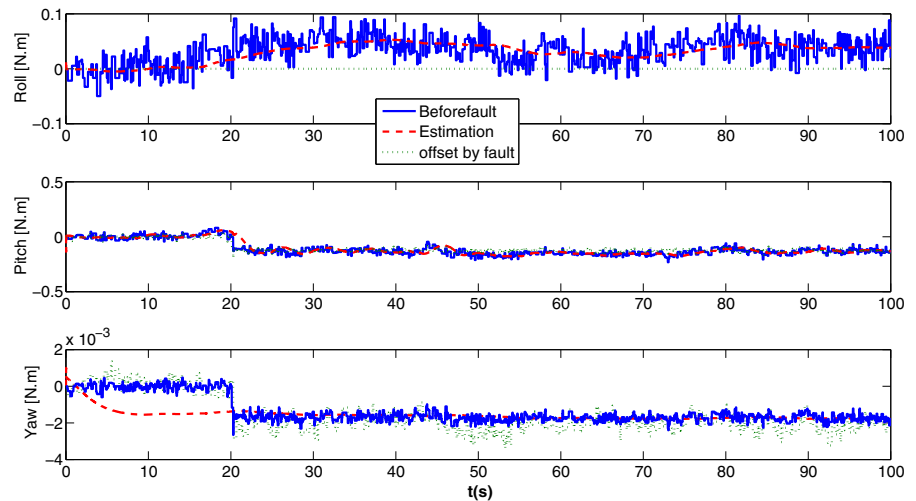
output offset by fault-U_e, and the control output offset by the fault-U_{offset} are shown in Fig. 10.

The ATO observer theoretically can make U_e converge to U_{offset}. From Fig. 10 we can see that it follows for pitch and yaw control, but U_e does not converge to U_{offset} for roll control, and converge to U_{bf} while U_{bf} is not equal to zero. So it means that the outside disturbance exists in the roll control.

The fault estimation for F1–F4 offset is shown in Fig. 11 and the comparison between the real value and its estimation for F1 offset by the fault is shown in Fig. 12.

As can be seen from Fig. 11, the estimations of F2, F3 and F4 are influenced by the disturbances. The estimations of F2, F3, F4 should be zero but they are not, and they sould be with a range

between −0.1 and 0.1 because of the disturbances. Although the result is not accurate, it is sufficient to isolate the faulty rotor.

As can be seen from the comparison between the real value of the fault offset F1 and its estimation by the ATO in Fig. 12, the ATO can estimate the fault offset value with a high accuracy.
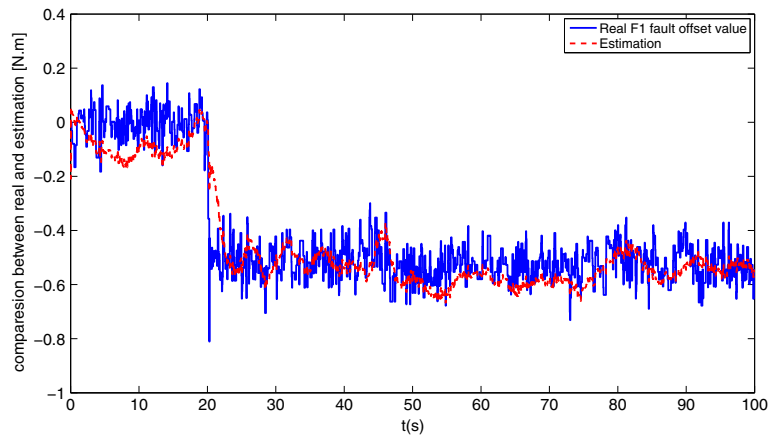
5.3 Optimized Robust FE Result

5.3.1 Unmodeled Optimization Result

The unmodeled optimization result for roll control is shown in Fig. 13. The offset value (green line) is zero, means that the fault injection into

Fig. 11 Fault estimation for F1–F4 with F1 fault
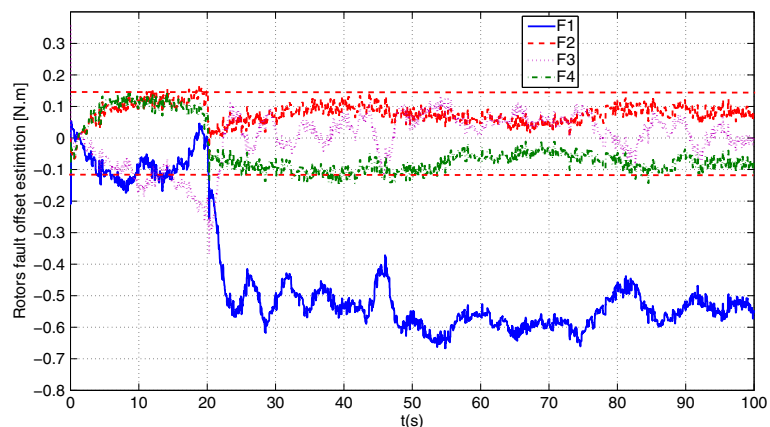
**Fig. 12** Fault estimation based on the ATO method

F1 doesn't affect the roll control. The control input of roll without fault (blue line) indicates a disturbance above zero but is not equal to zero. As can be seen from our former FE for the fault offset of roll control (red line), it can track this disturbance closely. So it means that the disturbance derives from the unmodeled factor instead of the fault effect. In order to compensate for this disturbance, the unmodeled factor is analyzed and the corresponding model terms are added to the observer model (named as M1). So, the optimized FE result for the fault offset of roll control (purple line) indicates to be nearly zero. It can be concluded that the unmodeled disturbance is well compensated for by the proposed optimization method.

5.3.2 Magnitude Order Unbalance Optimization Result

The magnitude order unbalance optimization result is shown in Fig. 14. The offset value of yaw (green line) peaks at the fault instant ($t = 20$ s), it means that the fault injection into the rotor 1 takes effects on the yaw control. The control input for yaw without fault (blue line) also peaks at $t = 20$ s which follows the offset value. As a result of magnitude order unbalances, our former FE for the fault offset of roll control (red line) cannot estimate the offset value correctly because it is not sensitive to the fault. With the proposed optimization data adjustment method (M2), it can track the offset value closely as can be seen from the
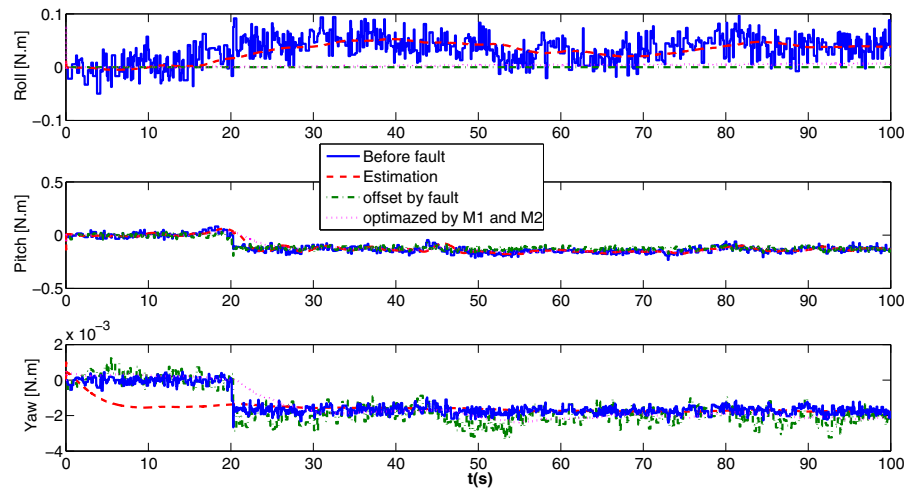
Fig. 13 Optimization for unmodelling in roll control by M1
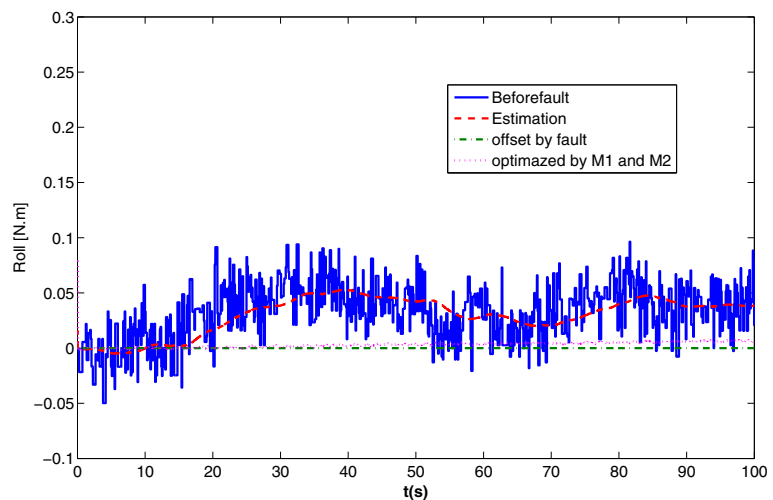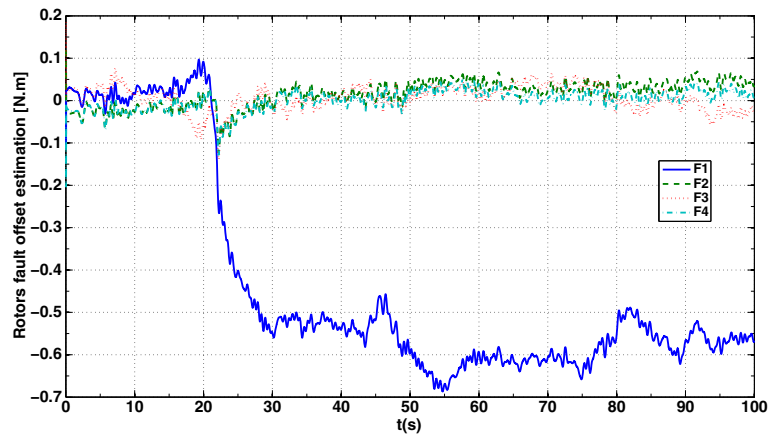
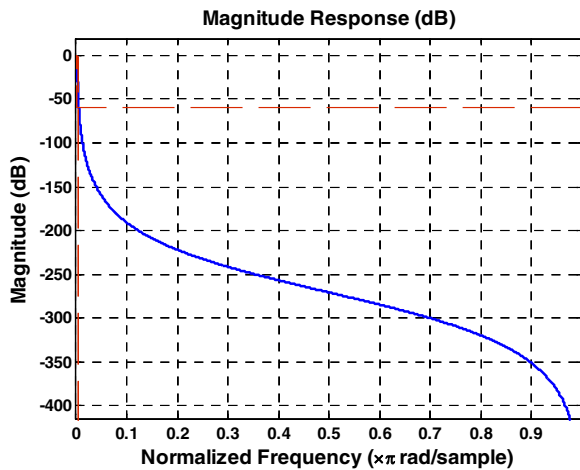**Fig. 14** Optimization for unmodelling errors in *yaw* control by M2
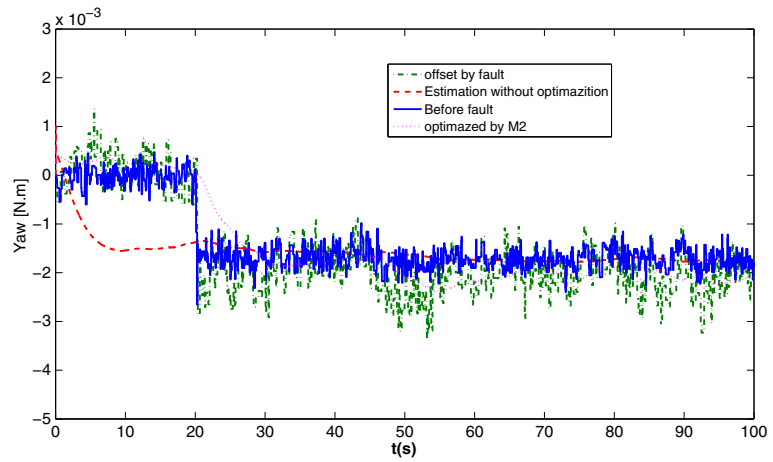
Fig. 15 Optimization FE results for *roll*, *pitch* and *yaw* control by M1 and M2

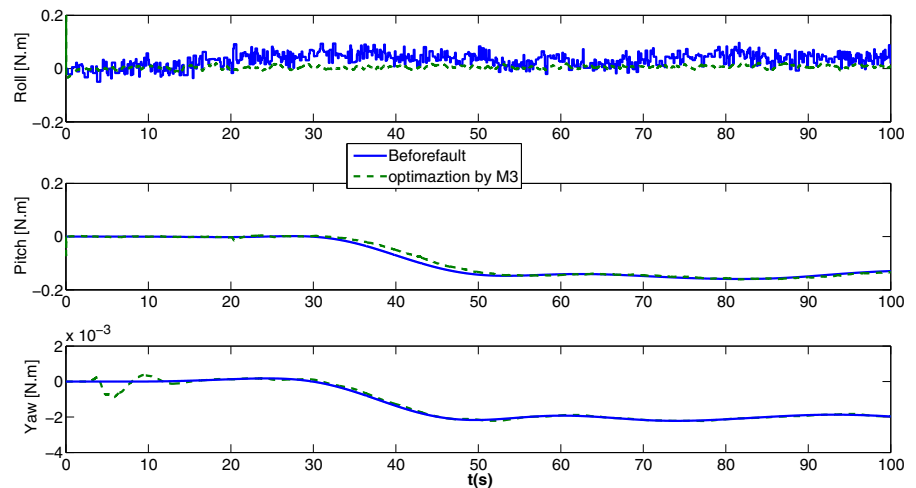**Fig. 16** Optimization FE results for 4 rotors F1–F4 by M1 and M2

Fig. 17 Frequency spectrum of the defined IIR filter

optimized FE for the fault offset of yaw control (purple line).

The optimization FE for roll, pitch, yaw controls by M1 and M2 is shown in Fig. 15 and the optimization FE for four rotors by M1 and M2 is shown in Fig. 16.

As can be seen from Fig. 16, the uncertainties are well compensated for by the proposed optimization method M1 and M2. Also, the FE for pitch can still track the fault offset value although the optimization is introduced. Comparing the optimized FE for 4 rotors shown in Fig. 16 with the former FE result shown in Fig. 11, it can be seen that the residuals for F2–F4 are well improved.

Fig. 18 Optimization FE results for *roll*, *pitch* and *yaw* control by M3

Fig. 19 Optimization FE results for the four rotors F1–F4 by M3
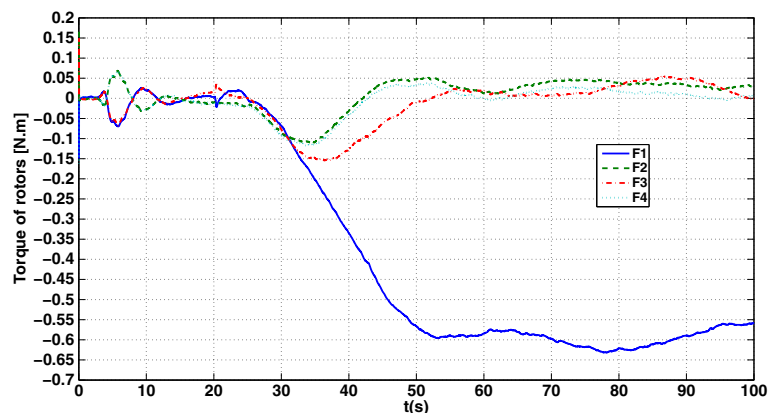
5.3.3 Denoising Optimization Result

In order to filter noises in the residuals, IIR low-pass filters with the pass frequencies 0.001–0.005 (normalized frequency) are used to filter the control input U1–U4(named as M3).The pass frequencies from 0.001 to 0.5 are tested. Based on the analysis of test result, the range (0.001–0.005) is more effective for the control signal and the IIR filter can respond faster because of its simple structure. The IIR filters frequencies spectrum character is shown in Fig. 17.

The optimized FE result for roll, pitch, yaw controls by M3 is shown in Fig. 18 and the optimized FE result for the four rotors using M3 is shown in Fig. 19.

As depicted in Fig. 18, if the filter is used to decrease the noise of pitch and roll control inputs, the optimized FE by M3 can track the filtered fault offset more closely. As shown from Fig. 19, the noises in the residuals (F1–F4) are filtered and the residuals F2–F4 are improved.

6 Conclusion

This paper proposed a robust FD scheme based on a novel ATO and optimization method for quadrotor faults with a real implementation on the real quadrotor. The proposed FD scheme can detect and isolate the fault. Also, based on a systemic robust optimization approach, faults can be estimated with an acceptable accuracy. Unlike former research work on FD for quadrotors, the proposed FD scheme based on the ATO can not only detect fault actuators, but also estimate the fault severity based on the real flight data. The experiment demonstrates effectiveness of the proposed method. Future work will consider AFTC control strategy based on FE result.

References

1. Freddi, A., Longhi, S., Monteriù, A.: A diagnostic thau observer for a class of unmanned vehicles. J. Intell. Robot. Syst. **67**, 1–13 (2012)
2. Freddi, A., Longhi, S., Monteriù, A.: A model-based fault diagnosis system for a mini-quadrotor. In: Proc. 2009 7th Workshop on Advanced Control and Diagnosis, pp. 19–20
3. Freddi, A., Longhi, S., Monteriu, A.: Actuator fault detection system for a mini-quadrotor. In: 2010 IEEE International Symposium on Proc. 2010 Industrial Electronics (ISIE), pp. 2055–2060
4. Yu, Y., Ding, X.: A quadrotor test bench for six degree of freedom flight. J. Intell. Robot. Syst. **68**, 323–338 (2012)
5. Vitzilaios, N.I., Tsourveloudis, N.C.: An experimental test bed for small unmanned helicopters. J. Intell. Robot. Syst. **54**, 769–794 (2009)
6. Abdolhosseini, M., Zhang, Y.M., Rabbath, C.A.: An efficient model predictive control scheme for an unmanned quadrotor helicopter. J. Intell. Robot. Syst. **70**, 27–38 (2013)
7. Mohammadi, M., Shahri, A.M.: Adaptive nonlinear stabilization control for a quadrotor UAV: theory, simulation and experimentation. J. Intell. Robot. Syst. **72**, 105–122 (2013)
8. Escareño, J., Salazar, S., Romero, H., Lozano, R.: Trajectory control of a quadrotor subject to 2D wind disturbances. J. Intell. Robot. Syst. **70**, 51–63 (2013)
9. Liu, H., Bai, Y., Lu, G., Shi, Z., Zhong, Y.: Robust tracking control of a quadrotor helicopter. J. Intell. Robot. Syst. (2013). doi:10.1007/s10846-013-9838-2
10. Tarhan, M., Altuğ, E.: EKF based attitude estimation and stabilization of a quadrotor UAV using vanishing points in catadioptric images. J. Intell. Robot. Syst. **62**, 587–607 (2011)
11. Rinaldi, F., Chiesa, S., Quagliotti, F.: Linear quadratic control for quadrotors UAVs dynamics and formation flight. J. Intell. Robot. Syst. **70**, 203–220 (2013)
12. Zhang, Y., Chamseddine, A.: Automatic flight control systems—latest developments. In: Fault Tolerant Flight Control Techniques with Application to a Quadrotor UAV Testbed, vol. Intech (2012)
13. Izadi, H.A., Zhang, Y., Gordon, B.W.: Fault tolerant model predictive control of quad-rotor helicopters with actuator fault estimation. In: Proc. 2011 Proceedings of the 18th IFAC World Congress, pp. 6343–6348 (2011)
14. Sadeghzadeh, I., Mehta, A., Zhang, Y., Rabbath, C.A.: Fault-tolerant trajectory tracking control of a quadrotor helicopter using gain-scheduled PID and model reference adaptive control. In: Proc. 2011 Annual Conference of the Prognostics and Health Management Society, pp. 25–29 (2011)
15. Zhang, Y., Jiang, J.: Bibliographical review on reconfigurable fault-tolerant control systems. Annu. Rev. Control **32**, 229–252 (2008)
16. Sobhani-Tehrani, E., Khorasani, K.: Fault diagnosis of nonlinear systems using a hybrid approach, vol. 383. Springer (2009)
17. Amoozgar, M.H., Chamseddine, A., Zhang, Y.: Experimental test of a two-stage kalman filter for actuator fault detection and diagnosis of an unmanned quadrotor helicopter. J. Intell. Robot. Syst. **70**, 107–117 (2013)
18. Qi, X., Theilliol, D., Qi, J., Zhang, Y., Han, J.: A literature review on fault diagnosis methods for manned and unmanned helicopters. In: International Conference on Proc. 2013 Unmanned Aircraft Systems (ICUAS), pp. 1114–1118 (2013)

19. Amoozgar, M.H., Chamseddine, A., Zhang, Y.M.: Experimental test of an interacting multiple model filtering algorithm for actuator fault detection and diagnosis of an unmanned quadrotor helicopter. In: ICIRA'12 Proceedings of the 5th International Conference on Intelligent Robotics and Applications, vol 1, pp. 473–482. Springer-Verlag Berlin, Heidelberg (2012)

20. Ma, L.: Development of fault detection and diagnosis techniques with applications to fixed-wing and rotary-wing UAVs. Master Degree dissertation, Concordia University (2011)

21. Ma, L., Zhang, Y.: DUKF-based GTM UAV fault detection and diagnosis with nonlinear and LPV models. In: Proc. 2010 Proceedings of the 6th ASME/IEEE International Conference on Mechatronic & Embedded Systems & Applications, pp. 375–380

22. Ma, L., Zhang, Y.M.: Fault detection and diagnosis for GTM UAV with dual unscented Kalman filter. In: Proc. 2010 AIAA Guidance, Navigation, and Control Conference, pp. 3204–3215

23. Ranjbaran, M., Khorasani, K.: Fault recovery of an under-actuated quadrotor Aerial Vehicle. In: 49th IEEE Conference on Proc. 2010 Decision and Control (CDC), pp. 4385–4392 (2010)

24. Cen, Z., Noura, H., Al Younes, Y.: Engineering implementation on fault diagnosis for quadrotors based on nonlinear observer. In: Proc. 2013 25th Chinese Control and Decision Conference (CCDC) (2013)

25. Cen, Z., Noura, H., Younes, Y.A.: Robust fault estimation on a real quadrotor UAV using optimized adaptive Thau observer. In: International Conference on Proc. 2013 Unmanned Aircraft Systems (ICUAS), pp. 550–556 (2013)

26. Sharifi, F., Mirzaei, M., Gordon, B.W., Zhang, Y.: Fault tolerant control of a quadrotor UAV using sliding mode control. In: Conference on Proc. 2010 Control and Fault-Tolerant Systems (SysTol), pp. 239–244 (2010)

27. Meng, L., Jiang, B., Xu, Y.: Observer-based robust fault diagnosis for a class of uncertain nonlinear systems. In: Proc. 2009 Control and Decision Conference, CCDC'09. Chinese, pp. 885–889 (2009)

28. Zhang, K., Jiang, B., Shi, P.: Adaptive observer-based fault diagnosis with application to satellite attitude control systems. In: Second International Conference on Proc. 2007 Innovative Computing, Information and Control, ICICIC'07, p. 508 (2007)